Eight-Planar-Monopole MIMO Circular Array Generating Eight Uncorrelated Waves for 6G Upper Mid-Band 8 x 8 MIMO Access Points

KIN-LU WONG[1,2], (Fellow, IEEE), YI-RONG CHEN[1], (Student Member, IEEE), and WEI-YU LI[3], (Member, IEEE)

[1]Department of Electrical Engineering, National Sun Yat-sen University, Kaohsiung 80424, Taiwan
[2]6G Communication and Sensing Research Center, National Sun Yat-sen University, Kaohsiung 80424, Taiwan
[3]Information and Communications Research Laboratories, Industrial Technology Research Institute, Hsinchu 31057, Taiwan

Corresponding author: Kin-Lu Wong (e-mail: wongkl@mail.nsysu.edu.tw).

ABSTRACT For next-generation or six-generation (6G) mobile communications, the 8 x 8 MIMO operation is envisioned for the user. In this case, as compared to the fifth-generation (5G) mid-band 4 x 4 MIMO operation, a much larger spectral efficiency can be expected for the user, which in turn will effectively increase the user-experienced data throughput with a fixed carrier bandwidth. For such applications, to transmit eight MIMO streams for the 6G 8 x 8 MIMO access point, a simple yet compact MIMO array formed by eight planar monopoles arranged in a circular array with radial metal walls to generate eight uncorrelated waves is presented in this study. The MIMO array operates in a wide band of 5.9-8.4 GHz, which covers the possible new 6G mobile bands in 5.925-7.125 GHz and 7.125-8.4 GHz. The targeted new 6G mobile bands are in the upper mid-band's lower frequency region, close to the 5G mid-band, and are expected to show similar rich multipath scattering as the 5G 4 x 4 MIMO operation. To verify it, we apply the proposed MIMO array to transmit eight MIMO streams for the 8 x 8 MIMO operation in a practical on-campus scenario and obtain a spectral efficiency of about 34 bps/Hz, which is about two times that of the 5G 4 x 4 MIMO operation. The results indicate that the proposed MIMO array is promising for applications in the 6G 8 x 8 MIMO system.

INDEX TERMS 6G upper mid-band MIMO antennas, 6G 8 x 8 MIMO systems, 8 x 8 MIMO access points, MIMO antennas, MIMO access-point antennas, planar monopole MIMO circular array

I. INTRODUCTION

It is well known that for 5G mobile communications, the 4 x 4 multi-input-multi-output (MIMO) operation in the mid-band such as the mobile bands in 3.3-5.0 GHz is applied [1]-[5]. It is further envisioned that for next-generation or 6G mobile communications, the higher-order MIMO such as the 8 x 8 MIMO system for the mobile device will be applied [1]-[3]. In this case, with the 8 x 8 MIMO operation, a much larger user-experienced spectral efficiency can be obtained, as compared to the 5G 4 x 4 MIMO operation. For such applications, eight isolated antennas at the transmitter or the access point to transmit eight MIMO streams are required.

In addition, for 6G mobile communications, the new frequency band in the upper mid-band in 7-24 GHz [1], [2] or 6-15 GHz [3], [6], [7] between the 5G mid-band in 3.3-5.0 GHz and the 5G millimeter-wave band in 24-52 GHz has

recently received much attention. This is owing to the upper mid-band's potential capability of supporting faster speeds and wider coverage [7], especially in its lower frequency region close to the 5G mid-band, such as in 5.925-7.125 GHz [3] or 6.425-7.125 GHz [8], or 7.125-8.4 GHz [2], [9]. This is because the lower the frequencies, the propagation path loss is generally lower and the multipath scattering is generally richer. The former leads to wider coverage, while the latter makes it possible to support the higher-order or 8 x 8 MIMO operation to achieve a much larger spectral efficiency than the 5G 4 x 4 MIMO operation, thereby achieving a much larger data throughput with a fixed carrier bandwidth for the user.

However, for the potential 6G 8 x 8 MIMO system, the required MIMO antennas are two times that of the 5G 4 x 4

MIMO system. Related studies on the multiport MIMO patch antennas backed by a ground plane have been reported for the 5G access-point applications, including the three-port patch antennas [10]-[13], the four-port patch antennas [14]-[18], and even the six-port patch antennas [19], [20]. These multiport patch antennas have a large ground plane so as to transmit multiple uncorrelated waves with increased antenna gain and also having a wide beamwidth in the front hemisphere above the ground plane. The antenna characteristics of increased antenna gain and wide beamwidth together can lead to stronger signal strength received at the receiver and richer multipath scattering in the MIMO environment between the transmitter and receiver. In this case, it becomes possible for the MIMO system to support higher-order MIMO operation, thereby achieving a much larger spectral efficiency for the user.

For such multiport patch antennas, in order to achieve enhanced isolation of any two ports over a wide operating band, various decoupling techniques have been applied, especially for the four-port and six-port patch antennas [14]-[20]. In [14], [15], [17], the decoupling techniques mainly include using external complex feed networks between the multiple ports, which however results in increased ohmic loss and decreased antenna efficiency. In [16], [18]-[20], the multiple isolated 90°- or 60°-resonant sectors are created in the radiating patch to radiate multiple uncorrelated waves over a wide band.

It is also noted that the multiple (three, four, or six) uncorrelated waves of the reported multiport patch antennas for access-point applications are mainly with broadside radiation patterns [10]-[20]. To radiate eight MIMO streams, two four-port patch antennas [19] were applied in an 8 x 8 MIMO system in a practical on-campus scenario [21]. Experimental results showed that the eight MIMO streams with mainly broadside radiation support a signal modulation of 64 Quadrate Amplitude Modulation (QAM) in a practical 8 x 8 MIMO scenario to have a spectral efficiency of about 34.8 bps/Hz [21], which is about two times that of the 5G 4 x 4 MIMO operation [4].

In this study, different from the reported multiport patch antennas with mainly broadside radiation [10]-[19], a simple yet compact MIMO array formed by eight planar monopoles (PMs) arranged in a circular array with radial metal walls to generate eight uncorrelated waves with monopolar-like radiation patterns is presented for the 6G 8 x 8 MIMO access-point application. The MIMO array covers the possible new 6G mobile bands of 5.9-8.4 GHz (35% fractional bandwidth covering 5.925-7.125 GHz [3], [8] and 7.125-8.4 GHz [2], [9]). The radial metal walls in the MIMO array lead to enhanced port isolation of the eight PMs therein, thereby achieving a compact array having a diameter of 63 mm (about 1.24λ at 5.9 GHz) only.

It is worthy to note that the MIMO array generates eight uncorrelated waves with monopolar-like radiation patterns mainly in the front hemisphere above the array's ground plane, similar to the case of multiport patch antennas with mainly broadside radiation [10]-[19]. In addition to different radiation characteristics (monopole-like vs. broadside radiation patterns), eight transmit MIMO streams in the 8 x 8 MIMO system requires only one proposed MIMO array, different from using two four-port patch antennas reported in [21].

In this study, we address the operating principle and design considerations of the eight-PM MIMO circular array, which is also fabricated and applied as the transmit antennas in a practical on-campus 8 x 8 MIMO operation [21], [22]. We also present the experimental results of the fabricated MIMO array and analyze its capability of supporting the 8 x 8 MIMO operation as compared to the case of using two four-port patch antennas to transmit eight MIMO streams in the MIMO system [21].

II. Eight-Planar-Monopole MIMO Circular Array

Fig. 1(a) shows the perspective view of the simple planar monopole MIMO circular array for 6G upper mid-band 8 x 8 MIMO access points. The corresponding top and side views are shown in Fig. 1(b). The circular array consists of eight planar monopoles (PM1-PM8 with Ports P1-P8) to radiate eight uncorrelated waves over a wide band covering 5.9-8.4 GHz (35% fractional bandwidth with respect to the center frequency at about 7.1 GHz). The eight planar monopoles have a same simple rectangular shape (10 mm x 12 mm) and are made of a 0.2 mm thick copper plate in this study.

Through a feed gap of 0.7 mm, each planar monopole is excited at the center of its bottom edge by a probe feed, which is connected to a 50 Ω SMA connector placed behind the ground plane. The total antenna height of the planar monopole above the ground plane is thus 10.7 mm (about 0.25λ at 7.1 GHz), thereby generating a resonant mode at about the desired center frequency. The relatively larger width (12 mm) of the planar monopole is for achieving a wide operating band to cover the desired operating band.

Note that the eight planar monopoles are placed along the array circle, with each one facing toward the array center. The circular array can also be divided into eight sectors of a 45-degree flare angle, with each sector accommodating one planar monopole. To obtain a compact array size for the eight planar monopoles having decreased coupling over the wide band, each 45-degree sector is chosen to have an arc length no larger than one-half wavelength at the lowest operating frequency (5.9 GHz in this study). That is, the array circle is considered to require no larger than four wavelengths at 5.9 GHz. Based on this array size consideration, the array circle is selected to have a diameter of 63 mm (about 1.24λ at 5.9 GHz), which has a length of about 198 mm or 3.9λ at 5.9 GHz.
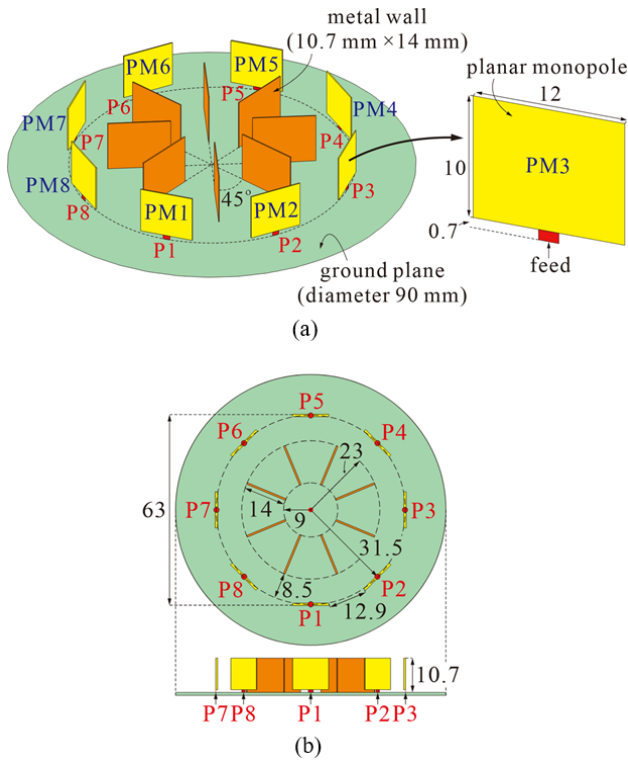
2

FIGURE 1. Geometry of the simple planar monopole MIMO circular array (PM1-PM8 with Ports P1-P8) for 6G upper mid-band 8 x 8 MIMO access points. (a) Perspective view. (b) Top and side views.
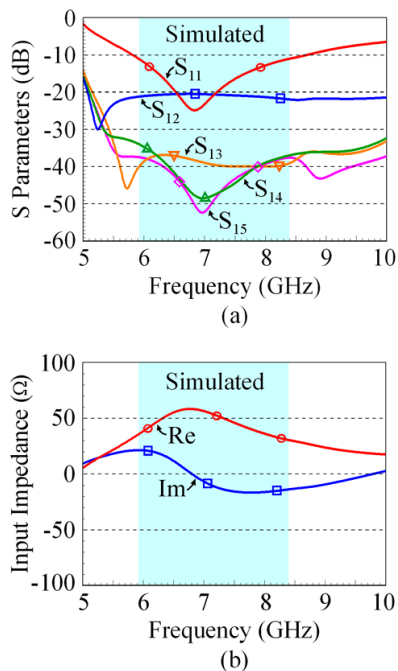

FIGURE 2. Simulated (a) S parameters and (b) input impedance of Port P1 in the MIMO array.
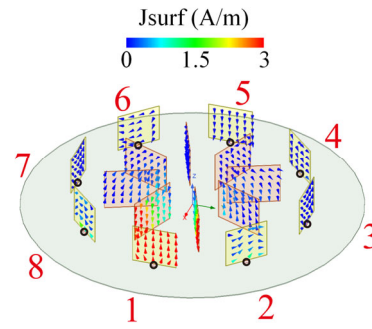

FIGURE 3. Simulated vector surface current distributions of Port P1 excited at 7.1 GHz with Ports P2-P8 terminated to 50 Ω.

Also, since the circular array is backed by a large ground plane of diameter 90 mm (about 1.77λ at 5.9 GHz), stronger radiation for the planar monopoles in the front hemisphere of the ground plane is expected, similar to the reported multiport patch antennas in [10]-[20].

To further obtain enhanced decoupling of the eight planar monopoles in the MIMO array, eight radial metal walls having same simple rectangular dimensions (height 10.7 mm above the ground plane, width 14 mm along the radial direction) and spaced to each other by 45 degrees are added inside the array. That is, each 45-degree sector locates a planar monopole facing the array center and has two metal walls along the sector's two radial side edge. By adjusting the distance of the metal walls to the array circle (selected to 8.5 mm in this study), enhanced port isolation with small effects on the impedance matching of the planar monopoles can be obtained.

Based on using the commercially available simulation tool HFSS [23] (High Frequency Structure Simulator) version 19.1, the performance of the MIMO array is analyzed. Fig. 2 shows the simulated S parameters and input impedance of Port P1 in the MIMO array. Owing to the symmetric structure of the MIMO array, the corresponding results of Ports P2-P8 are same as those of Port P1.

The colored frequency region in the figure indicates 5.925-8.4 GHz which covers the possible new 6G mobile bands of 5.925-7.125 GHz [3], [8] and 7.125-8.4 GHz [2], [9]. The simulated S parameters indicate that the planar monopole can cover the desired operating bands with the impedance matching less than -10 dB (see the S_{11} curve) and the port isolation larger than 20 dB for two nearby ports [see the S_{12} (= S_{18}) curve] or even larger than 33 dB for other two ports [see the S_{13} (= S_{17}), S_{14} (= S_{16}), and S_{15} curves in Fig. 2(a)].

The good impedance matching over the wide band is related to the smooth variation in the input impedance, in which a zero reactance near the targeted center frequency at 7.1 GHz is observed [see Fig. 2(b)]. That is, the planar monopole with the selected dimensions successfully generates a quarter-wavelength resonant mode to cover the desired wide band.
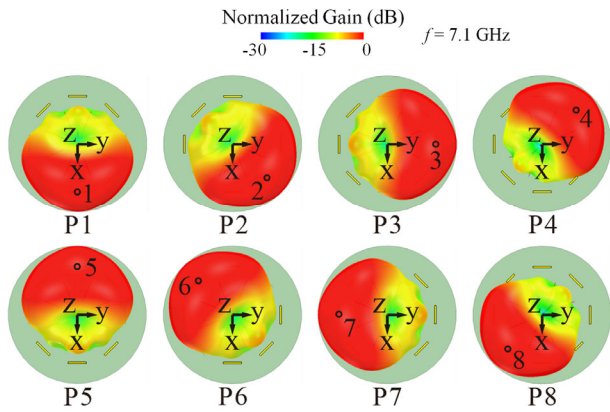
FIGURE 4. Simulated three-dimensional (3-D) normalized total-power radiation patterns seen from the *z* direction (array center) of Ports P1-P8 at 7.1 GHz.
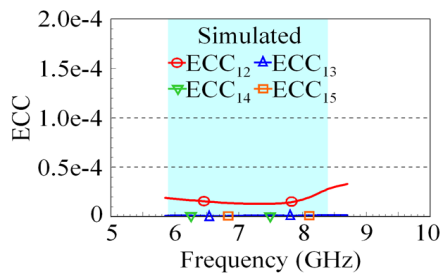

FIGURE 5. Simulated envelope correlation coefficients (ECC$_{mn}$) based on the far-field electric fields of the two waves generated by PM*m* and PM*n* in the MIMO array.

FIGURE 6. Simulated (a) antenna efficiency and (b) antenna gain of Port P1 in the MIMO array.

FIGURE 7. Simulated total active reflection coefficient (TARC) of Ports P1-P8 excited with same excitation phases in the MIMO array.

The simulated vector surface current distributions in the PM1 for Port P1 excited at 7.1 GHz are also seen to be along the upright direction above the ground plane (see Fig. 3). That is, the resonant frequency is mainly determined by the planar monopole length above the ground plane (10.7 mm here). By varying the planar monopole length, the resonant mode can be conveniently adjusted.

From the simulated normalized total-power radiation patterns seen from the *z* direction (array center) of Ports P1-P8 at 7.1 GHz (Fig. 4), it is seen that each radiating wave covers a wide area or has a wide beamwidth along the array circle. This characteristic can be advantageous for the eight radiating waves to provide rich multipath scattering in the MIMO environment between the transmitter and receiver. Very low envelope correlation coefficients (ECC$_{mn} < 10^{-4}$) based on the far-field electric fields of the two waves [24] generated by PM*m* and PM*n* in the MIMO array are also seen (Fig. 5). This indicates that the array can provide eight uncorrelated waves for MIMO operation.

Fig. 6 shows the simulated antenna efficiency and antenna gain of Port P1. The simulated antenna efficiency includes the mismatching loss and is larger than 90% over the desired wide band. The corresponding antenna gain varies in 5.7-8.2 dBi. The relatively larger antenna gain at higher frequencies is mainly because the effective ground plane size in wavelength is larger with increasing frequencies.
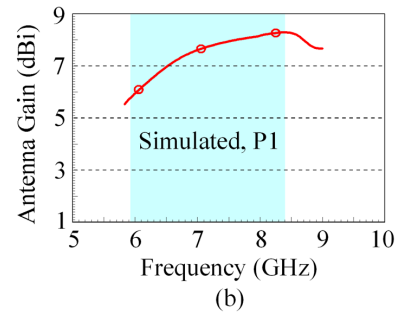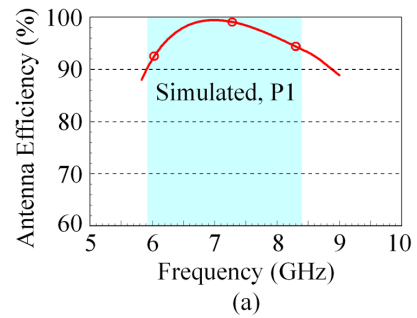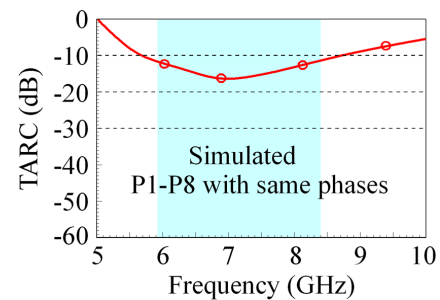
To consider the eight planar monopoles excited at the same time for transmitting eight MIMO streams in practical applications, Fig. 7 shows the simulated total active reflection coefficient (TARC) [19], [20], [25] of Ports P1-P8 excited with same excitation phases in the MIMO array. Over the desired wide band, the TRAC is seen to be less than -10 dB. This is largely because Ports P1-P8 have high port isolation as seen in Fig. 2.

The simulated mean effective gain (MEG) [26] of Port P1 in the MIMO array is presented in Fig. 8. The MEG is obtained under the assumption of uniform incident wave condition and is slightly varied from -3.1 to -3.5 dB over the wide band. Also, all Ports (Ports 1 to 8) have the same MEG owing to their symmetric structure in the MIMO array. That is, all eight ports have the same ratio of the average received power to the average power received by a reference antenna in the same propagation environment [27], which is expected to be advantageous for MIMO operation.
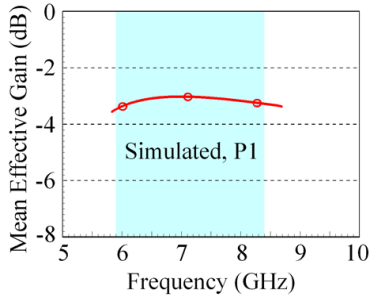
4

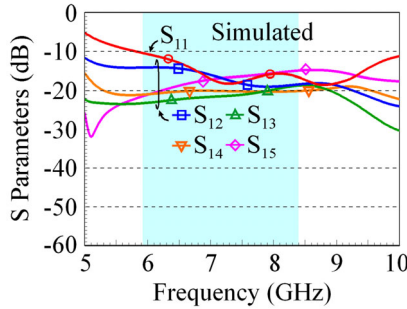**FIGURE 8.** Simulated mean effective gain (MEG) of Port P1 in the MIMO array.

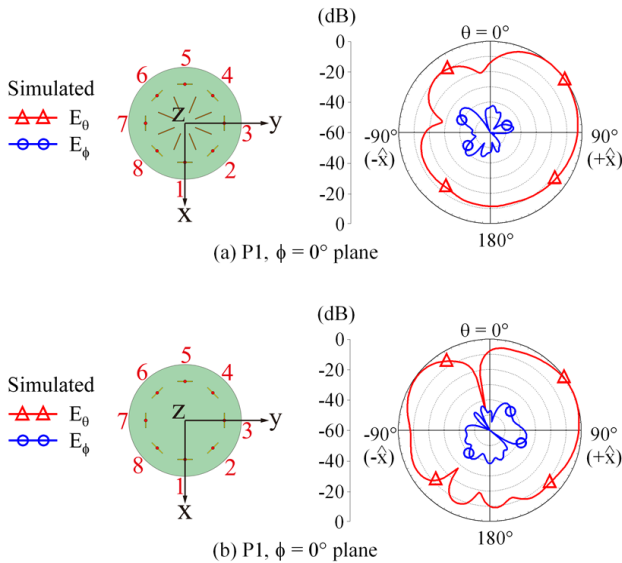**FIGURE 9.** Simulated *S* parameters of Port P1 in the MIMO array without the radial metal walls.

FIGURE 10. Simulated normalized radiation patterns at 7.1 GHz in the radial plane along the centerline (the $\phi = 0°$ plane) of Port P1. (a) Proposed MIMO array. (b) The case without radial metal walls.

FIGURE 11. Simulated *S* parameters of Port P1 for the radial metal walls placed with various distances (*a*) to the array circle. (a) S_{11}. (b) S_{12} (= S_{18}), S_{13} (= S_{17}). (c) S_{14} (= S_{16}), S_{15}. Other parameters are same as in Fig. 1.

In addition, it is seen in Fig. 10 that the radial metal walls make the radiation patterns of the planar monopoles tilted from the array center toward the array circle. That is, the monopole-like radiation pattern of each planar monopole is modified to be stronger toward the direction of its nearby ground edge [see Fig. 10(a) vs. Fig. 10(b)]. This characteristic may also account for the very low ECCs between all the radiating waves shown in Fig. 5.

III. Parametric Study

For finely adjusting the performance of the MIMO array, a parametric study on the radial metal walls and planar monopoles is presented. Fig. 11 shows the simulated *S* parameters of Port P1 for the radial metal walls placed with various distances (*a*) to the array circle. Results of the distance *a* varied from 6.5 mm to 10.5 mm are shown. The S_{11} are given in Fig. 11(a), the S_{12} (= S_{18}) and S_{13} (= S_{17}) are in Fig. 11(b), and the S_{14} (= S_{16}) and S_{15} are in Fig. 11(c).

Effects of the radial metal walls are also discussed. Fig. 9 shows the simulated *S* parameters of Port P1 in the MIMO array without the radial metal walls. The transmission coefficients of two nearby ports (S_{12}) and other two ports (S_{12}, S_{14}, S_{15}) are all much larger than their corresponding results of the case with radial metal walls [see Fig. 2(a)]. That is, the presence of the radial metal walls can lead to enhanced port isolation.
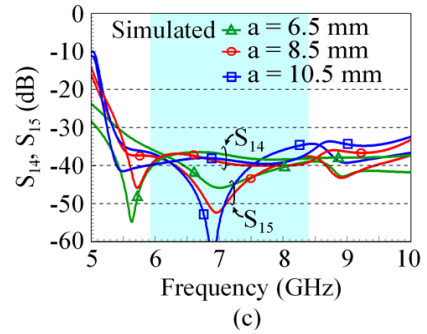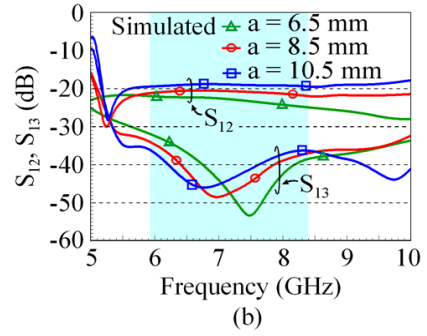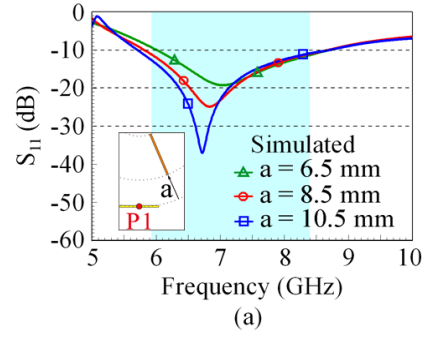
5

FIGURE 12. Simulated *S* parameters of Port P1 for various widths (*b*) of the radial metal walls. (a) S_{11}. (b) S_{12} (= S_{18}), S_{13} (= S_{17}). (c) S_{14} (= S_{16}), S_{15}. Other parameters are same as in Fig. 1.
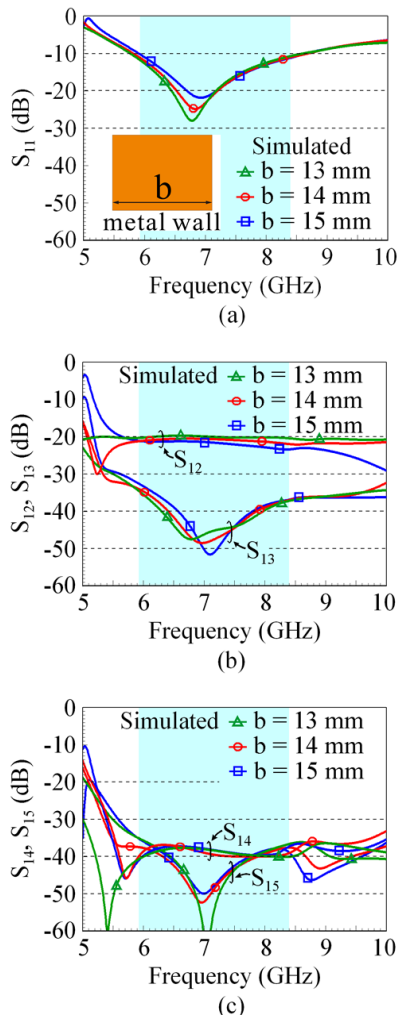
FIGURE 13. Simulated *S* parameters of Port P1 for various heights (*c*) of the radial metal walls. (a) S_{11}. (b) S_{12} (= S_{18}), S_{13} (= S_{17}). (c) S_{14} (= S_{16}), S_{15}. Other parameters are same as in Fig. 1.

When the radial metal walls are closer to the array circle, that is, closer to the planar monopoles, larger effects on the S_{11} or the impedance matching are seen and better port isolation for two nearby ports (the S_{12}) or two ports spaced by one planar monopole (the S_{13}) are also observed. The port isolation for two ports spaced by two or more planar monopoles is slightly affected. By varying the distance *a* (selected to be 8.5 mm here), balanced performance on the input impedance and port isolation can be adjusted.

Fig. 12 shows the simulated *S* parameters of Port P1 for various widths (*b*) of the radial metal walls. The width *b* varied from 13 mm to 15 mm is analyzed. Note that the distance of the metal walls to the array circle is fixed (8.5 mm here) and a larger width means the metal walls are extended toward the array center. Results indicate that a larger width causes stronger effects on the impedance matching of the planar monopole [see the S_{11} in Fig. 12(a)].
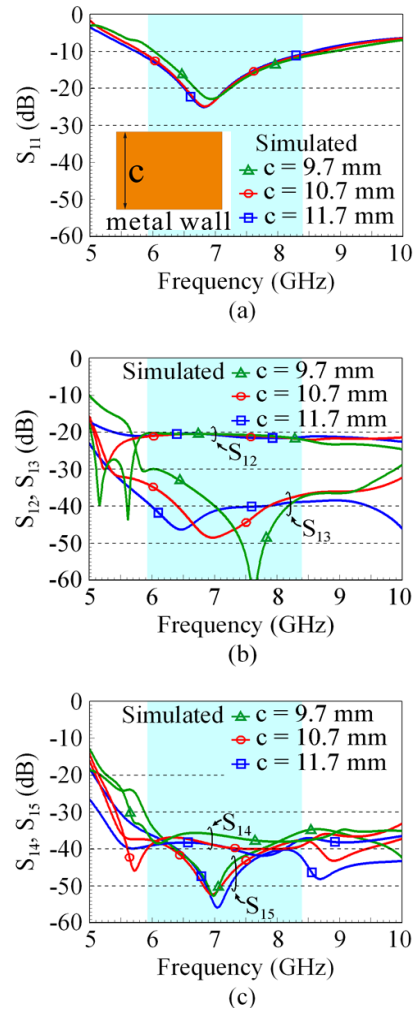
For the port isolation, relatively very small effects are observed [see Fig. 12(b) and (c)]. Thus, when the distance *a* in Fig. 11 is chosen, further adjustment on the impedance matching with the port isolation generally not to be affected, the width *b* can be varied.

Fig. 13 shows the simulated *S* parameters of Port P1 for various heights (*c*) of the radial metal walls. The height *c* varied from 9.7 mm to 11.7 mm is studied. Results indicate that when the height *c* is slightly varied with respect to the that of the planar monopole above the ground plane (10.7 mm here), small effects on the impedance matching and port isolation are seen. For convenience, the height *c* is chosen to be same as the height of the planar monopole in this study.

The parameters of the planar monopoles are studied in Figs. 14 and 15. The simulated *S* parameters of Port P1 as a function of the planar monopole width (*d*) are analyzed in Fig. 14. Results of the width *d* varied from 10 mm to 14 mm are shown. When a larger width *d* is selected, better impedance matching is seen [see Fig. 14(a)], while the port

6

isolation of two nearby ports is slightly degraded around 20 dB [see the S_{12} in Fig. 14(b)]. The port isolation of other two ports is still better than about 33 dB [see the S_{13}, S_{14}, S_{15} in Fig. 14(b) and (c)].
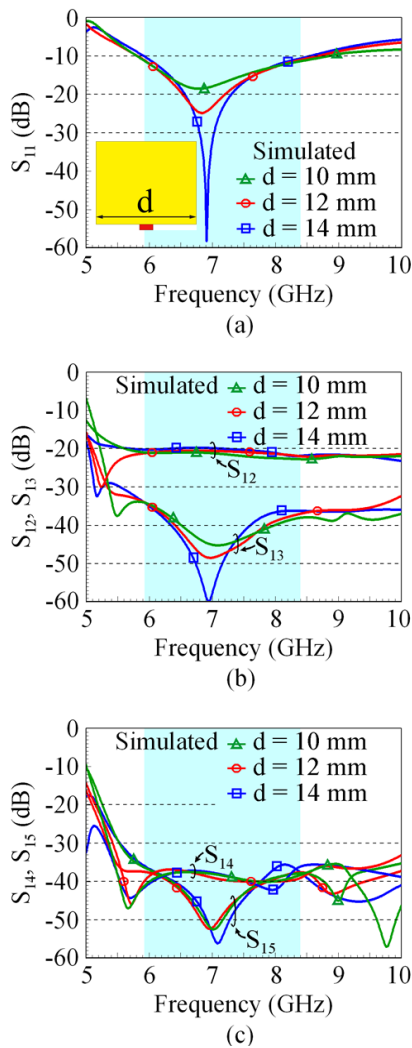

(a)

(b)

(c)

FIGURE 14. Simulated *S* parameters of Port P1 as a function of the planar monopole width (*d*). (a) S_{11}. (b) S_{12} (= S_{18}), S_{13} (= S_{17}). (c) S_{14} (= S_{16}), S_{15}. Other parameters are same as in Fig. 1.

Fig. 15 shows the simulated *S* parameters of Port P1 as a function of the planar monopole length (*e*). Results of the length *e* to be 9.5 mm, 10 mm, and 10.5 mm are shown. Since the length *e* mainly determines the resonant frequency of the excited quarter-wavelength resonant mode, a larger length *e* causes the resonant mode to lower frequencies [see Fig. 15(a)]. On the other hand, the port isolation is almost not affected [see Fig. 15(b) and (c)].

Fig. 16 shows the simulated *S* parameters of Port P1 as a function of the feed gap (*g*). By adjusting the feed gap *g*, the effective capacitance between the planar monopole and ground plane will be varied. This in turn will vary the input reactance seen at the feed port, therefore causing variations in

the impedance matching [see Fig. 16(a)]. On the other hand, the port isolation between any two ports is almost not affected [see Fig. 16(b) and (c)]. Based on the parametric study, one can finely adjust the impedance matching and port isolation of the planar monopoles in the MIMO array.
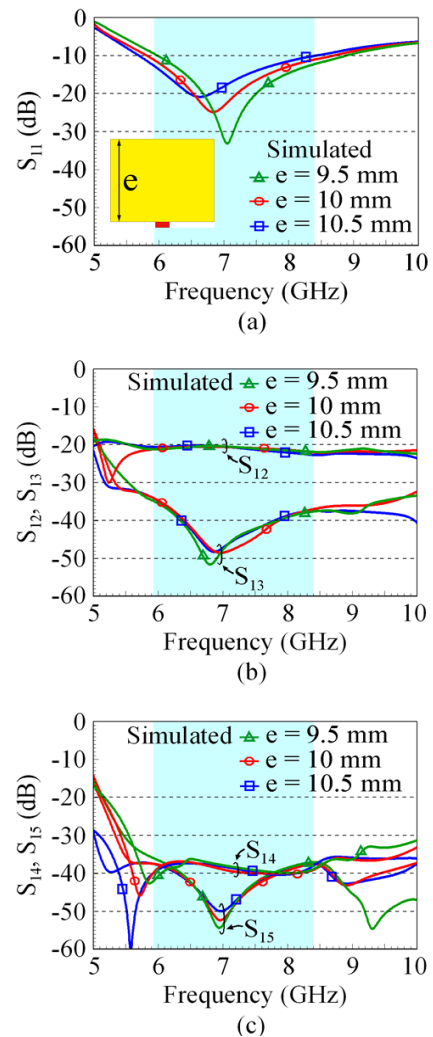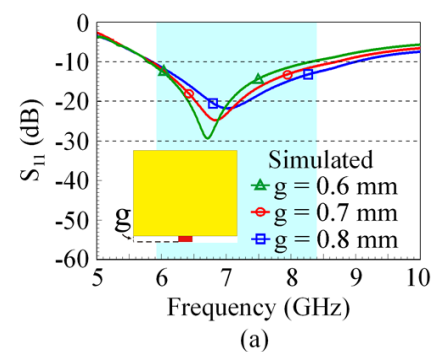

(a)

(b)

(c)

FIGURE 15. Simulated *S* parameters of Port P1 as a function of the planar monopole length (*e*). (a) S_{11}. (b) S_{12} (= S_{18}), S_{13} (= S_{17}). (c) S_{14} (= S_{16}), S_{15}. Other parameters are same as in Fig. 1.
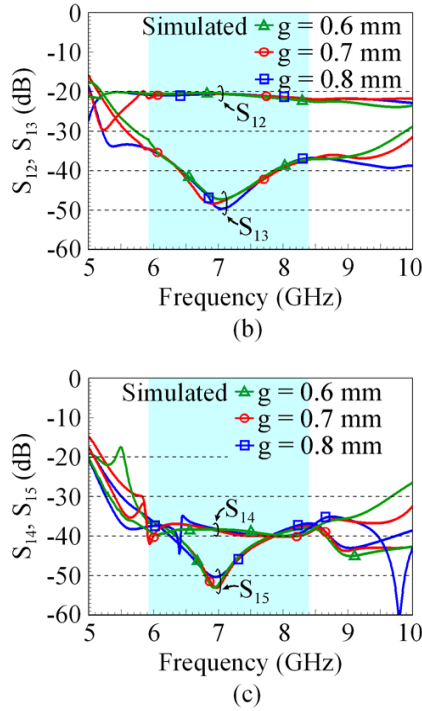

(a)

(b)

(c)

FIGURE 16. Simulated *S* parameters of Port P1 as a function of the feed gap (*g*). (a) S_{11}. (b) S_{12} (= S_{18}), S_{13} (= S_{17}). (c) S_{14} (= S_{16}), S_{15}. Other parameters are same as in Fig. 1.

IV. EXPERIMENTAL RESULTS OF THE FABRICATED MIMO ARRAY

The fabricated MIMO array shown in Fig. 17 was tested. The measured reflection coefficients of Ports P1-P8 of the fabricated MIMO array are shown in Fig. 18(a) and (b). The corresponding transmission coefficients of two adjacent ports and two ports spaced by one planar monopole are respectively shown in Fig. 19(a)-(d). Those for two ports spaced by two and three planar monopoles are shown in Fig. 20(a)-(c). The measured *S* parameters generally agree with the corresponding simulated results. Over the desired wide band of 5.9-8.4 GHz, the impedance matching of the eight planar monopoles in the fabricated MIMO array is less than -10 dB. The port isolation is larger than 20 dB for two adjacent ports and even larger than about 30 dB for other two ports spaced by at least one planar monopole.

The radiation characteristics of the MIMO array are tested in the far-field anechoic chamber (see the experimental setup in Fig. 21) with the Great Circle Test method [28] applied to obtain the three-dimensional (3-D) radiation patterns. Figs. 22 and 23 respectively show the measured antenna efficiency and antenna gain of the eight planar monopoles in the MIMO array. The measured and simulated results are in good agreement. The measured antenna efficiency is larger than about 88% and the antenna gain is varied in about 5.4-8.2 dBi over the wide operating band.
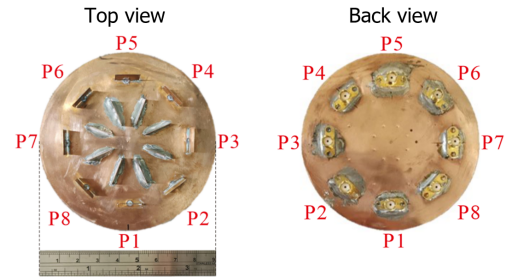
FIGURE 17. Photos of the fabricated MIMO array.

(a)

(b)
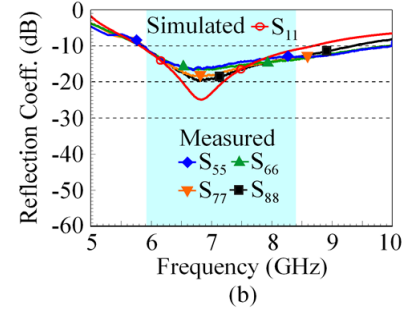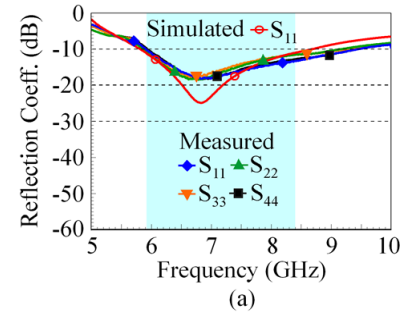
FIGURE 18. Measured reflection coefficients. (a) Ports P1-P4. (b) Ports P5-P8.

(a)

(b)

(c)

(d)
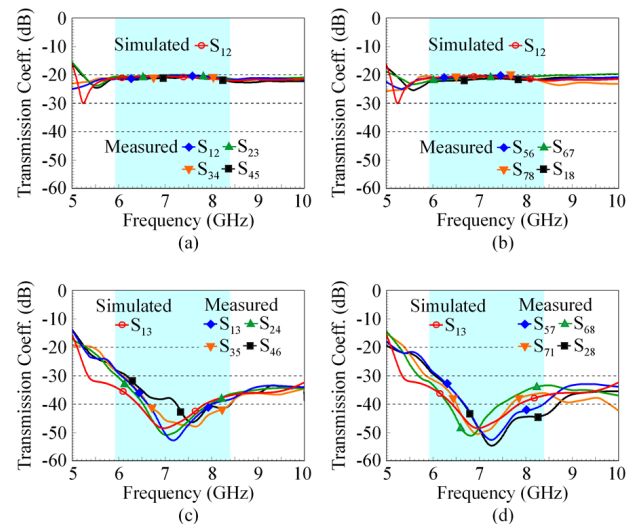
FIGURE 19. Measured transmission coefficients. (a) Two adjacent ports (S_{12}, S_{23}, S_{34}, S_{45}). (b) Two adjacent ports (S_{56}, S_{67}, S_{78}, S_{18}). (c) Two ports spaced by one planar monopole (S_{13}, S_{24}, S_{35}, S_{46}). (d) Two ports spaced by one planar monopole (S_{57}, S_{68}, S_{71}, S_{28}).

8

FIGURE 20. Measured transmission coefficients. (a) Two ports spaced by two planar monopoles (S_{14}, S_{25}, S_{36}, S_{47}). (b) Two ports spaced by two planar monopoles (S_{58}, S_{61}, S_{72}, S_{38}). (c) Two ports spaced by three planar monopoles (S_{15}, S_{26}, S_{37}, S_{48}).

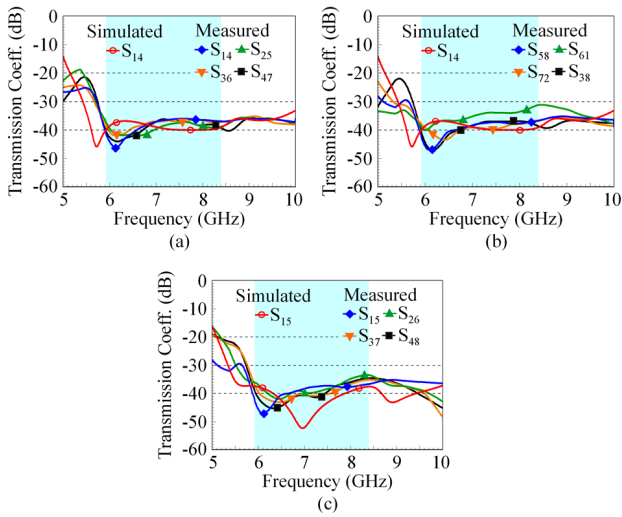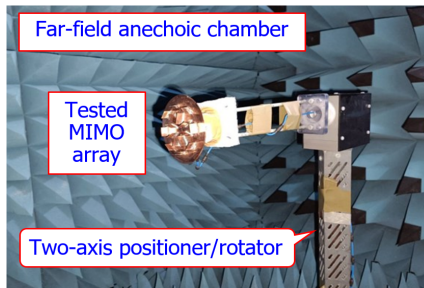**FIGURE 21.** The fabricated MIMO array tested in a far-field anechoic chamber.
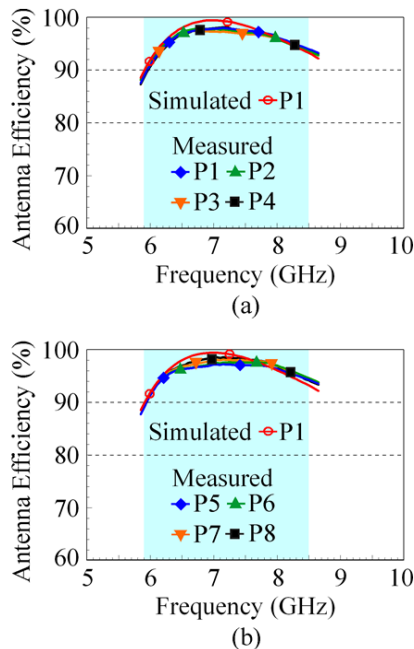
FIGURE 22. Measured antenna efficiency. (a) Ports P1-P4. (b) Ports P5-P8.
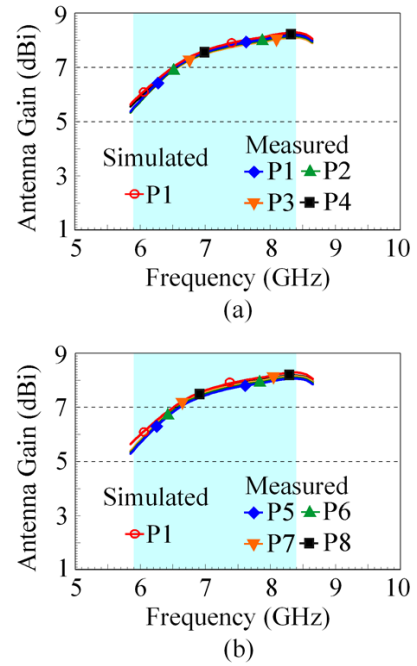
FIGURE 23. Measured antenna gain. (a) Ports P1-P4. (b) Ports P5-P8.
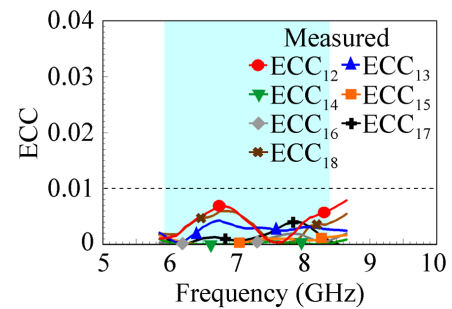
FIGURE 24. Calculated ECCs based on the measured electric fields of the 3-D radiation patterns of two ports between Port P1 and Ports P2-P8.

Fig. 24 shows the calculated ECCs based on using the measured electric fields of the 3-D radiation patterns [24], [26] of two ports between Port P1 and Ports P2-P8. The obtained maximum ECC values are only 0.007. The results indicate that the generated waves can be considered to be uncorrelated, which is advantageous for MIMO applications.

Figs. 25 and 26 shows the measured normalized radiation patterns at 7.1 GHz for Ports P1-P8 in the radial plane of their respective feed to the array center. The radiation patterns for Port P1 in the $\phi = 0^o$ plane, Port P2 in the $\phi = 45^o$ plane, Port P3 in the $\phi = 90^o$ plane, and Port P4 in the $\phi = 135^o$ plane are respectively shown in Fig. 25(a), (b), (c), and (d). Those for Port P5 in the $\phi = 180^o$ plane, Port P6 in the $\phi = 225^o$ plane, Port P7 in the $\phi = 270^o$ plane, and Port P8 in the $\phi = 315^o$ plane are plotted in Fig. 26(a), (b), (c), and (d).

9

FIGURE 25. Measured and simulated normalized radiation patterns at 7.1 GHz for Ports P1-P4 in the radial plane along their respective feed and the array center. (a) Port P1. (b) Port P2. (c) Port P3. (d) Port P4.

FIGURE 26. Measured and simulated normalized radiation patterns at 7.1 GHz for Ports P5-P8 in the radial plane along their respective feed and the array center. (a) Port P5. (b) Port P6. (c) Port P7. (d) Port P8.

The measured radiation pattern for each port generally agrees with its corresponding simulated pattern, which is also adde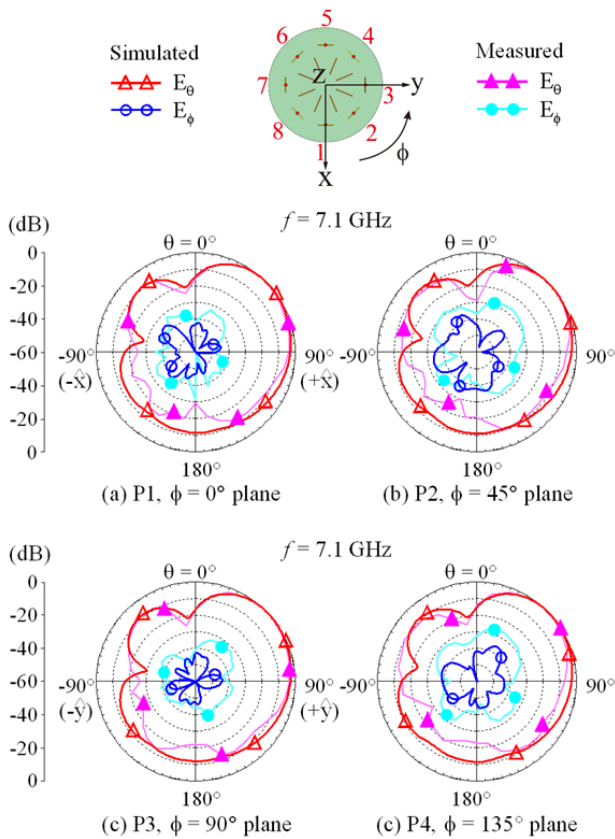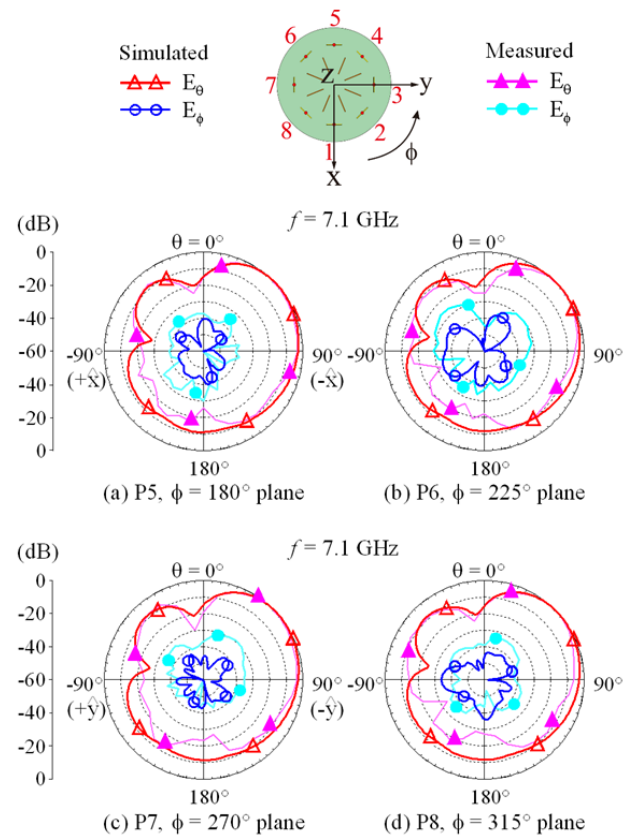d in each figure for comparison. From the measured results, the fabricated MIMO array can generate eight uncorrelated monopole-like waves with their radiation patterns stronger near the ground edge. The application of the fabricated MIMO array for the 8 x 8 MIMO operation is then studied in the next section.

V. 8 x 8 MIMO TESTING OF THE FABRICATED MIMO ARRAY

Fig. 27 shows the 8 x 8 MIMO system testbed at National Sun Yat-sen University (NSYSU) [21], [22]. The fabricated MIMO array at the transmitter (Tx) transmits 8 MIMO streams. The 8-port MIMO patch antenna [21] is applied at the receiver (Rx) to receive the 8 MIMO streams. Note that the 8-port MIMO patch antenna is circular in shape (diameter 46 mm) and is mounted on a ground plane of 150 mm x 70 mm (a size of typical modern smartphone) [21].

The 8 x 8 MIMO testing is conducted in the open concave space in front of the entrance of the Electrical Engineering (EE) Department building, NSYSU [see Fig. 28]. The MIMO operation is to simulate the Tx outdoor-Rx indoor scenario. That is, the Tx is considered to be located at an outdoor access point to transmit 8 MIMO streams into the indoor space in which the Rx or the smartphone with the 8-port MIMO patch antenna is used to receive the transmitted 8 MIMO streams. The 8 x 8 MIMO system testbed can provide the measured channel capacity in the MIMO environment and the data throughput received at the Rx. The detailed experimental setup of the 8 x 8 MIMO system tested was described in [21].

Note that two orientations of the receive antennas with respect to the transmit antennas are tested. The first one is the receive antennas facing the transmit antennas in a line-of-sight (LOS) orientation with a distance of 9 meters. The second one is the receive antennas moved 35 degrees away from the LOS direction, with the transmit antennas fixed; that is, a non-LOS orientation. Both orientations have a same distance of 9 meters between the receive and transmit antennas.

10

IEEE *Access*

Multidisciplinary ⋮ Rapid Review ⋮ Open Access Journal

TABLE 1. Measured results of the 8 x 8 MIMO system using the fabricated MIMO array as eight transmit antennas operated in the 7.1 GHz band (7.025-7.125 GHz). The MIMO testbed and testing scenario are shown in Figs. 27 and 28.

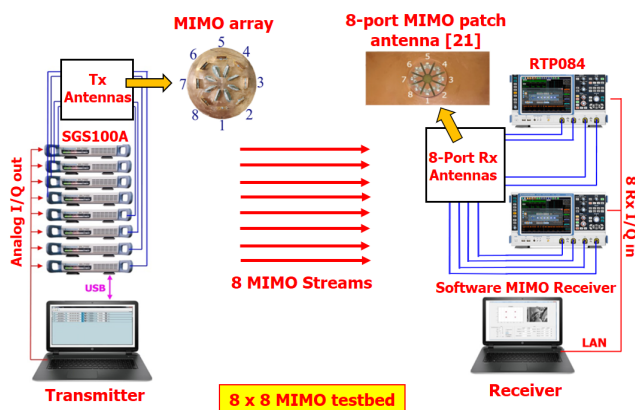| f_0 = 7.075 GHz (7.025-7.125 MHz), 8 × 8 MIMO, Tx outdoor-Rx indoor Scenario, Distance 9 m, Signal Modulation: 64 QAM			
Transmitter side: Tx1: Fabricated MIMO array transmitting 8 MIMO streams Tx2: Two 4-port MIMO patch antennas [21] **Receiver side**: Rx: 8-Port MIMO patch antenna [21] receiving 8 MIMO streams **MIMO scenario**: Open concave space in front of the entrance of the Electrical Engineering Department building, NSYSU			
Tx-Rx pair	Tx1-Rx	Tx1-Rx	Tx2-Rx [21]
Tx-Rx Orientation (Tx fixed)	Line-Of-Sight (LOS)	Non-LOS (35°)	Line-Of-Sight
Measured Signal Noise Ratio (dB) of the 8-Port MIMO Patch Antenna	22.4, 24.7, 24.0, 23.0 22.4, 22.4, 22.5, 24.4 (8 Ports at Rx, Average SNR = 23.4 dB)	25.1, 23.7, 25.4, 25.7 24.7, 23.2, 24.0, 25.6 (8 Ports at Rx, Average SNR = 24.8 dB)	26.4, 25.4, 26.3, 26.7 26.8, 25.8, 27.7, 25.9 (8 Ports at Rx, Average SNR = 26.4 dB)
Measured 8 x 8 MIMO Capacity	44.5 bps/Hz	46.1 bps/Hz	42.8 bps/Hz
Uncoded Bit Error Rate	0.024	0.021	0.013
Measured 8 x 8 MIMO Throughput	3438 Mbps	3449 Mbps	3476 Mbps
8 x 8 MIMO Spectral Efficiency	34.38 bps/Hz	34.49 bps/Hz	34.76 bps/Hz

FIGURE 27. The 8 x 8 MIMO testbed at National Sun Yat-sen University (NSYSU) [2]. The fabricated MIMO array is applied as the transmit (Tx) antennas. The 8-port MIMO patch antenna [21] is used as the receive (Rx) antennas at the receiver.

FIGURE 28. The 8 x 8 MIMO testing with Tx outdoor/Rx indoor scenario in the open concave space in front of the entrance of the EE department building, NSYSU. (a) Panoramic view for two orientations with Tx fixed (Rx LOS to Tx and Rx non-LOS to Tx). (b) Setup positions for Rx LOS to Tx; Rx non-LOS to Tx also with a distance of 9 meters.

The MIMO testing is conducted in the 7.1 GHz band (7.025-7.125 GHz, center frequency 7.075 GHz, bandwidth 100 MHz), which is being considered as a promising new mobile band for the global mobile communications [8]. For comparison, two Tx-Rx pairs of Tx1-Rx and Tx2-Rx are tested. The fabricated MIMO array in this study is the Tx1 antennas, while two 4-port MIMO patch antennas used in [21] are the Tx2 antennas. The 8-port MIMO patch antenna also used in [21] is the Rx antennas. Both Tx1 and Tx2 are fed with the same input power and the transmitted MIMO streams are with 64 QAM signal modulation.

Table 1 lists the measured signal noise ratio (SNR) of the 8 ports in the Rx antennas, measured 8 x 8 MIMO capacity in the testing scenario, the uncoded bit error rate (BER), the measured 8 x 8 MIMO throughput, and the corresponding spectral efficiency. The BER is the ratio of the error data received at the receiver to the total transmitted data. The

1

MIMO throughput is the correct data received at the receiver and is obtained by the total transmitted data times (1-BER). The spectral efficiency is the MIMO throughput divided by the operating bandwidth (100 MHz here).

From the results, the average SNR of the 8 receive ports in the Tx1-Rx LOS pair is lower by about 3 dB as compared to that of Tx2-Rx pair. This may be owing to the lower radiating field strength at the broadside direction of the Tx1 (the MIMO array with eight monopole-like radiation patterns) as compared to the Tx2 (the two 4-port MIMO patch antennas with eight near-broadside radiation patterns [19]). However, the Tx1-Rx LOS pair has a larger MIMO capacity than the Tx2-Rx pair (44.5 vs. 42.8 bps/Hz). This is largely because the Tx1 with monopole-like radiation patterns and in a circular array mounted vertically to the surface of the testing environment can lead to stronger multipath scattering in the testing scenario.

In this case, although the SNR is lower in the Tx1-Rx LOS pair, the obtained uncoded BER is comparable to that of the Tx2-Rx pair. Since the obtained uncoded BER is much less than 0.1, the zero coded BER can generally be obtained in practical communications [22]. This indicates that both pairs can support the 8 x 8 MIMO operation with the 64 QAM signal modulation. The measured throughput and spectral efficiency of the Tx1-Rx pair (LOS) are respectively 3438 Mbps and 34.38 bps/Hz, which are very close to those of the Tx2-Rx pair.

In addition, the results of the Tx1-Rx non-LOS pair also show comparable or even slightly larger spectral efficiency to that of the Tx1-Rx LOS pair (34.49 vs. 34.38 bps/Hz). This may be because the Rx with 35 degrees away from the LOS direction can have stronger received power than in the LOS direction (average SNR 24.8 dB vs. 23.4 dB shown in the table), owing to the Tx1's monopole-like radiation characteristic.

In addition, in the testing scenario, it is very likely to have similar strong multipath scattering in both the non-LOS and LOS directions, also owing to the Tx1 with monopole-like radiation patterns and the circular array mounted vertically to the surface of the testing environment. Thus, for both the Tx1-Rx non-LOS and LOS pairs, similar good 8 x 8 MIMO performance is obtained. The obtained results indicate that the fabricated MIMO array with monopole-like radiation patterns is applicable in the 8 x 8 MIMO system in the 7.1 GHz band.

VI. CONCLUSION

A compact MIMO circular array formed by eight simple planar monopoles has been shown to be promising for the 6G upper mid-band 8 x 8 MIMO access-point applications. The MIMO array can transmit eight uncorrelated waves in a wide band of 5.9-8.4 GHz to cover 5.925-7.125 GHz [3], [8] and 7.125-8.4 GHz [2], [9], which are the possible new 6G mobile bands in the upper mid-band. The operating principle

and design considerations of the MIMO array have been addressed in this study. Successful application of the fabricated MIMO array as the transmit antennas in the 8 x 8 MIMO system in an on-campus Tx outdoor-Rx indoor scenario has been demonstrated. The spectral efficiency of about 34 bps/Hz in the 7.1 GHz band has been obtained, which is about two times that of the 5G 4 x 4 MIMO operation in the 3.5 GHz band. The proposed MIMO array is expected to find applications in the 6G 8 x 8 MIMO system.

REFERENCES

[1] (Jan. 7, 2022). *MediaTek 6G Vision Whitepaper.* [Online]. Available: https://www.mediatek.com/whitepapers/6g

[2] (May 1, 2022). *Samsung 6G Whitepaper: Spectrum Expanding the Frontier.* [Online]. Available: https://cdn.codeground.org/nsr/downloads/ researchareas/2022May_6G_Spectrum.pdf

[3] (Nov. 1, 2021). *6G: The Next Horizon, Huawei 6G Research Team.* [Online]. Available: https://www.huawei.com/en/technology-insights/ future-technologies/6g-the-next-horizon

[4] I. R. R. Barani, K. L. Wong, Y. X. Zhang, and W. Y. Li, "Low-profile wideband conjoined open-slot antennas fed by grounded coplanar waveguides for 4 x 4 5G MIMO operation," *IEEE Trans. Antennas Propag.*, vol. 68, pp. 2646-2657, Apr. 2020.

[5] L. Chang and H. Wang, "Miniaturized wideband four-antenna module based on dual-mode PIFA for 5G 4×4 MIMO applications," *IEEE Trans. Antennas Propag.*, vol. 69, pp. 5297-5304, Sep. 2021.

[6] K. Lee, J. Kim, E. W. Jin, and K. S. Kim, "Extreme massive MIMO for upper-mid band 6G communications," *2022 13th International Conf. on Information and Communication Technology Convergence (ICTC)*, Jeju Island, Korea, Oct. 2022, pp. 997-999.

[7] (Mar. 1, 2022). *"New Frontiers of Partnerships," Remarks of the U.S. FCC Chairwoman J. Rosenworcel in Mobile World Congress, Barcelona, Spain.* [Online]. Available: https://www.fcc.gov/document/chairwoman-rosenworcel-remarks-mobile-world-congress-2022

[8] (Nov. 6, 2019). *WRC-19 (World Radiocommunication Conference 2019) Report. Key Outcomes of the WRC-19.* [Online]. Available: https://www.itu.int/en/itunews/Documents/2019/2019-06/2019_ ITUNews06-en.pdf

[9] (May 17, 2022). *2022 Spectrum development, National Spectrum Development Association.* [Online]. Available: https://www.nsma.org/wp-content/uploads/9.-State-of- the-Spectrum_Remaley-Conway.pdf

[10] K. L. Wong, C. M. Chou, Y. J. Yang, and K. Y. Wang, "Multipolarized wideband circular patch antenna for fifth-generation multi-input-multi-output access-point application," *IEEE Antennas Wireless Propag. Lett.*, vol. 18, pp. 2184-2188, Oct. 2019.

[11] C.-Y. Chiu, B. K. Lau, and R. D. Murch, "Bandwidth enhancement technique for broadside tri-modal patch antenna," *IEEE Open J. Antennas Propag.*, vol. 1, pp. 524-533, 2020.

[12] C.-Y. Chiu, S. Shen, B. K. Lau, and R. D. Murch, "The design of a trimodal broadside antenna element for compact massive MIMO arrays: utilizing the theory of characteristic modes," *IEEE Antennas Propag. Mag.*, vol. 62, pp. 46-61, Dec. 2020.

[13] K. L. Wong and G. L. Yan, "Wideband three-port equilateral triangular patch antenna generating three uncorrelated waves for 5G MIMO access points," *IEEE Access.*, vol. 10, pp. 893-899, 2022.

[14] D. Manteuffel and R. Martens, "Compact multimode multielement antenna for indoor UWB massive MIMO," *IEEE Trans. Antennas Propag.*, vol. 64, pp. 2689-2697, Jul. 2016.

[15] W. Su, Q. Zhang, S. Alkaraki, Y. Zhang, X.-Y. Zhang, and Y. Gao, "Radiation energy and mutual coupling evaluation for multimode MIMO antenna based on the theory of characteristic mode," *IEEE Trans. Antennas Propag.*, vol. 67, pp. 74-84, Jan. 2019.

[16] K. L. Wong, H. Y. Jiang, and W. Y. Li, "Decoupling hybrid metal walls and half-wavelength diagonal open-slots based four-port square patch antenna with high port isolation and low radiation correlation for 2.4/5/6 GHz WiFi-6E 4 x 4 MIMO access points," *IEEE Access*, vol. 10, pp. 81296-81308, 2022.

[17] N. Peitzmeier, T. Hahn, and D. Manteuffel, "Systematic design of multimode antennas for MIMO applications by leveraging symmetry," *IEEE Trans. Antennas Propag.*, vol. 70, pp. 145-155, Jan. 2022.

[18] K. L. Wong, J. Z. Chen, and W. Y. Li, "Four-port wideband annular-ring patch antenna generating four decoupled waves for 5G multi-input-multi-output access points," *IEEE Trans. Antennas Propag.*, vol. 69, pp. 2946-2951, May 2021.

[19] K. L. Wong, X. Q. Ye, and W. Y. Li, "Wideband four-port single-patch antenna based on the quasi-TM$_{1/2,1/2}$ mode for 5G MIMO access-point application," *IEEE Access*, vol. 10, pp. 9232-9240, 2022.

[20] K. L. Wong, Z. W. Tso, and W. Y. Li, "Very-wide-band six-port single-patch antenna with six uncorrelated waves for MIMO access points," *IEEE Access*, vol. 10, pp. 69555-69567, 2022.

[21] K. L. Wong, H. C. Kao, and W. Y. Li, "Wideband low-profile eight-port eight-wave annular-ring patch antenna based on using eight dual-shorted dual-resonant ring sectors for 8 x 8 MIMO mobile devices," *IEEE Access*, vol. 11, pp. 18-32, 2023.

[22] K. L. Wong, "5G/B5G multi-Gbps antennas for user terminals and their throughput verification," *Proc. 2020 Asia Pacific Microwave Conference (APMC)*, Hong Kong, China, pp. 366-368.

[23] (Mar. 1, 2022). *3D High Frequency Electromagnetic Simulation Software, ANSYS HFSS.* [Online]. Available: https://www.ansys.com/products/electronics/ansys-hfss

[24] A. Iqbal, A. Altaf, M. Abdullah, M. Alibakhshikenari, E. Limiti, and S. Kim, "Modified U-shaped resonator as decoupling structure in MIMO antenna," *Electronics*, vol. 9, Article 1321, 2020.

[25] M. Manteghi and Y. Rahmat-Samii, "Multiport characteristics of a wide-band cavity backed annular patch antenna for multipolarization operations," *IEEE Trans. Antennas Propag.*, vol. 53, pp. 466-474, Jan. 2005.

[26] M. S. Sharawi, "Printed multi-band MIMO antenna systems and their performance metrics," *IEEE Antennas Propag. Mag.*, vol. 55, pp. 218-232, Oct. 2013.

[27] A. A. Glazunov, A. F. Molisch, and F. Tufvesson, "Mean effective gain of antennas in a wireless channel," *IET Microw. Antennas Propag.*, vol. 3, Iss. 2, pp. 214-227, 2009.

[28] Y. Okano and K. Cho, "Antenna measurement system for mobile terminals," *NTT DoCoMo Technical Journal*, vol. 9, no. 2, pp. 43-50, 2007.

KIN-LU WONG (Fellow, IEEE) received the B.S. degree in electrical engineering from the National Taiwan University, Taipei, Taiwan, in 1981, and the M.S. and Ph.D. degrees in electrical engineering from Texas Tech University, Lubbock, TX, USA, in 1984 and 1986, respectively.

From 1986 to 1987, he was a visiting scientist with the Max-Planck-Institute for Plasma Physics in Munich, Germany. Since 1987, he has been with the Electrical Eng. Dept., National Sun Yat-sen University (NSYSU), Kaohsiung, Taiwan, where he became a Professor in 1991. From 1998 to 1999, he was a Visiting Scholar with the ElectroScience Laboratory, The Ohio State University, Columbus, Ohio, USA. He was elected to be a Sun Yat-sen Chair Professor at NSYSU, in 2005, a Distinguished Chair Professor at NSYSU, in 2017, and the National Chair Professor of Ministry of Education (MOE) of Taiwan, in 2016. He also served as the Chairperson for the Electrical Eng. Dept. from 1994 to 1997, the Vice President for Research Affairs from 2005 to 2007, and the Senior Vice President at NSYSU, from 2007 to 2012. He is currently the Director of 6G Communication and Sensing Research Center funded by the Ministry of Education. He is also a National Chair Professor of Ministry of Education, a Distinguished Researcher of National Science and Technology Council, and a Distinguished Chair Professor with NSYSU. He has authored more than 580 refereed journal papers and 300 conference articles and has personally supervised 57 graduated Ph.D. He holds over 300 patents, including 103 U.S. patents. He is the author of *Design of Nonplanar Microstrip Antennas and Transmission Lines* (Wiley, 1999), *Compact and Broadband Microstrip Antennas* (Wiley, 2002), and *Planar Antennas for Wireless Communications* (Wiley, 2003). His published articles have been cited over 34,800 times with an H-index of 87 in Google Scholar.

Dr. Wong served or currently serves as an IEEE AP-S AdCom member, an IEEE Transactions on Antennas and Propagation Track Editor/Associate Editor, an IEEE Transactions on Antennas and Propagation Paper Awards Committee member, and an AP-S Field Awards Committee member. He received the Outstanding Research Award three times (1995, 2000, and 2002) from the Taiwan National Science Council. He also received the Outstanding Electrical Engineering Professor Award (2003) from the Institute of Electrical Engineers of Taiwan and the Outstanding Engineering Professor Award (2004) from the Institute of Engineers of Taiwan. In 2008, the research achievements on handheld device antennas of NSYSU Antenna Lab led by him was selected to be top 50 scientific achievements of the Taiwan Ministry of Science and Technology in past 50 years (1959-2009). He was a recipient of the 2010 Outstanding Research Award of Pan Wen Yuan Foundation and selected as top 100 Honor of Taiwan by Global Views Monthly, in August 2010, for his contribution in mobile antenna researches. He was also a recipient of the Academic Award (2012) from the Taiwan Ministry of Education and the Outstanding Distinguished Researcher Award (2013) from the Taiwan Ministry of Science and Technology. He and his graduate students have been awarded the Best Paper Award (APMC Prize) from 2008 APMC, the Best Student Paper Award/Young Scientist Award from 2007 ISAP, 2008 APMC, 2009 ISAP, 2010 ISAP, 2012 ISAP, and 2016 ISAP. His graduate students also won the first prize of 2007 and 2009 Taiwan National Mobile Handset Antenna Design Competition. He was awarded the Best Associate Editor two times (2015, 2016) for the IEEE Transactions on Antennas and Propagation. He was also a PE7 Panel Member of 2015, 2017, and 2019 European Research Council Advanced Grant Panel, and a Chief Consultant of the Institute of Antenna Engineers of Taiwan. He also served as the Chair for the judge panel (2014-2023) of the National Communication Antenna Design Competition organized by the Taiwan Ministry of Economics. He served as the General Chairs for 2012 APMC, 2014 ISAP, and 2016 APCAP held at Kaohsiung, Taiwan. He was elected as a Thomson Reuters Highly Cited Researcher in both 2014 and 2015 and also elected as an Elsevier Most Cited Researcher in 2015. In 2022, He was selected by Research.com to be ranked #99 in Full World Ranking and #1 in Full Taiwan Ranking in the 2022 Edition of Ranking of Top 1000 Scientists in the field of Electronics and Electrical Engineering. He is a Thomson Reuters Highly Cited Researcher and an Elsevier Most Cited Researcher

YI-RONG CHEN (Student Member, IEEE) received the B.S. degree in electrical engineering from the National Kaohsiung University of Science and Technology, Kaohsiung, Taiwan, in 2022. He is currently pursuing the M.S. degree at National Sun Yat-Sen University, Kaohsiung, Taiwan. His main research interests include high-density MIMO antennas for next-generation access-point and mobile-device applications.

WEI-YU LI (Member, IEEE) was born in Taipei, Taiwan, in 1981. He received the B.S. degree in electrical engineering from Feng Chia University, Taichung, Taiwan, in 2004, and the M.S. and Ph.D. degrees in electrical engineering from the National Sun Yat-sen University (NSYSU), Kaohsiung, Taiwan, in 2006 and 2009, respectively.

After graduated from NSYSU, in 2009, he has been with the Information and Communication Research Laboratories (ICL) of Industrial Technology Research Institute (ITRI), Hsinchu, Taiwan, participating and leading advanced research for development of emerging wireless antenna technologies. From April to October 2012, he was as an Exchange Guest Researcher with the National Institute of Information and Communications Technology (NICT), Tokyo, Japan. He is currently a technology manager at ITRI. He has authored and co-authored 34 refereed journal papers and 40 conference articles. He holds over 70 patents, including U.S., Taiwan, China, and EU patents. His published articles have been cited over 1,600 times with an H-index of 23 in Google Scholar.

Dr. Li served as an International Steering Committee Member of 2019-2022 ISAP and an AdCom Member of the Institute of Antenna Engineers of Taiwan (2014, 2015, and 2018-2022). He also served as a member of the Judge Panel (2014 to 2023) for the National Terminal Antenna Design Competition organized by the Taiwan Ministry of Economics. He received the Young Scientist Award from 2007 ISAP and the Best Paper Award (APMC Prize) from 2008 APMC. He has been a principal investigator or co-principal investigator of many research projects in ITRI and has received numerous recognitions, including the First Prize of the Outstanding Research Award of ITRI, in 2010, the Solar Industrial Award (SIA) of Europe, in 2011, the Outstanding Innovation Award of ITRI, in 2013, the Second Prize of the Outstanding Research Award of ITRI, in 2014, the 2015 Research and Development 100 Award Finalist of the U.S., the Outstanding Innovation Award of ITRI, in 2017, the First Prize of the Outstanding Industrialization Award of ITRI, in 2017, the Second Prize of the Outstanding Industrialization Award of ITRI, in 2020, and the Third Prize of the Outstanding Industrialization Award of ITRI, in 2021. He also received the Outstanding Lecturer Award of ITRI, in 2013, and the International Paper Award of ICL of ITRI, in 2020. He is the Chair of IEEE AP-S Tainan Chapter (2021-2022).